Experimental and theoretical studies of the effect of mass on the dynamics of gas/organic-surface energy transfer

William A. Alexander and B. Scott Day
Department of Chemistry, Virginia Tech, Blacksburg, Virginia 24061-0212, USA

H. Justin Moore and T. Randall Lee
Department of Chemistry, University of Houston, Houston, Texas 77204-5003, USA

John R. Morris and Diego Troya[a)]
Department of Chemistry, Virginia Tech, Blacksburg, Virginia 24061-0212, USA

(Received 13 August 2007; accepted 25 October 2007; published online 4 January 2008)

The effect of mass on gas/organic-surface energy transfer is explored via investigation of the scattering dynamics of rare gases (Ne, Ar, and Kr) from regular (CH_3-terminated) and ω-fluorinated (CF_3-terminated) alkanethiol self-assembled monolayers (SAMs) at 60 kJ/mol collision energy. Molecular-beam scattering experiments carried out in ultrahigh vacuum and molecular-dynamics simulations based on high-accuracy potentials are used to obtain the rare-gases' translational-energy distributions after collision with the SAMs. Simulations indicate that mass is the most important factor in determining the changes in the energy exchange dynamics for Ne, Ar, and Kr collisions on CH_3- and CF_3-terminated SAMs at 60 kJ/mol collision energy. Other factors, such as changes in the gas-surface potential and intrasurface interactions, play only a minor role in determining the differential dynamics behavior for the systems studied. © *2008 American Institute of Physics*.
[DOI: 10.1063/1.2815327]

I. INTRODUCTION

A detailed characterization of the collision dynamics between gas-phase species and organic surfaces is essential to understanding the interfacial behavior of organic surfaces. Early molecular-beam scattering studies by Nathanson and co-workers investigated the dynamics of energy transfer in collisions of atomic gases and small molecules (Ne, Ar, Xe, SF_6, CH_4, NH_3, and H_2O) with liquid organic surfaces.[1–4] They found the scattered gases' final translational-energy distributions to be bimodal, with a low-energy thermal desorption component well characterized by a Boltzmann distribution at the surface temperature. This low-energy component is attributed to collision events in which the gas traps for some time on the surface and eventually desorbs thermally. The high-energy component of the distribution was ascribed to impulsive collision events in which the gas' brief encounter with the surface does not allow thermalization. The consensus in the field has since been that in most cases the dynamics of gas/organic-surface collisions can be understood as the competition between two main mechanisms: Impulsive scattering and trapping desorption. While impulsive scattering is reminiscent of direct gas-phase collisions, trapping enables enhanced gas/surface energy transfer and allows for thermal accommodation of the gas on the surface.

Among the liquid surfaces investigated in the work of Nathanson and co-workers are squalane (2,6,10,15,19,23-hexamethyltetracosane) and perfluoropolyether (PFPE). These two liquids served as models of hydrocarbon and fluorocarbon surfaces, respectively. Comparison of the scattering properties of these two liquids revealed that gas/surface energy transfer depends critically on liquid composition, and only secondarily on the varying chemical and physical properties of the probe gases.[1,2] Overall, the results show that energy transfer from the scattered gases to the squalane surface is more efficient than with the PFPE surface. Moreover, while an increase in projectile mass led to an increase in energy transfer, the underlying surface effects persisted.[2,4] Those efforts have further shown that energy transfer is insensitive to gas identity for gases with similar masses; high incident energy Ne, CH_4, NH_3, and H_2O give similar overall energy transfer profiles on the same organic surface for nonpolar surfaces.[3,4] Even SF_6, with 15 vibrational and 3 rotational modes available in which to deposit energy during collision, closely mimics the energy transfer behavior of Xe.[2]

More recently, Perkins and Nesbitt, via high-resolution direct infrared absorption spectrometry and laser dopplerimetry techniques, have studied CO_2 scattering from the same squalane and PFPE liquid surfaces and their results agree well with the findings of Nathanson and co-workers.[5] Product-energy distributions were well characterized by separation into thermal desorption and impulsive scattering components, and overall energy transfer from CO_2 to the squalane surface was found to be more efficient than transfer to PFPE. These experiments also showed that energy transfer in the impulsive scattering channel is highly efficient and nearly the same from both surfaces, despite differences in surface properties and a marked difference in overall energy transfer to the two surfaces.[5] This agrees well with the finding that thermal roughening of the surfaces does not alter energy transfer in impulsive events.[6]

Although the previous experiments indicate that the

[a)]Electronic mail: troya@vt.edu.

chemical and physical structures of the organic liquid affect gas/surface energy transfer, the independent effects of mass, structure, and chemical properties of the surface on the energy transfer dynamics remain to be deciphered. The specific role of gas and surface masses has been an important component in understanding collision dynamics since the early developments of hard-cube models of gas-surface scattering.[7] The hard-cube model is based on the assumption that the component of the gas' momentum parallel to the surface is conserved during collision. The perpendicular component is altered via an impulsive hard-wall collision with a cube vibrating at the surface temperature. Borne out from the model is the fact that energy transfer is maximal when the gas/surface mass ratio, $\mu = m_{\mathrm{gas}}/m_{\mathrm{surface}}$, equals 1. Under the assumption of energy and momentum conservation, the fractional energy transfer to the surface for a normal incidence angle can be written as $\Delta E/E_i = 4\mu/(\mu+1)^2$, where ΔE is the change in energy of the gas, and E_i is the incident gas energy. By fitting the value of the mass ratio μ to experimental data, this relationship has been used to obtain an "effective" surface mass, which gives some idea of the collective response of the surface in collisions. The hard-cube model and its various extensions have been widely applied to describe experimentally observed trends in gas/surface scattering from metals and other inorganic surfaces.[8,9] While the model performs well for smooth, hard surfaces—giving quantitative agreement with experiment for systems in which its use is optimal[10]—it is not well known if the same descriptions of collision dynamics are applicable to softer, organic solids, such as polymers. Saecker and Nathanson have applied a hard-cube description to the above-mentioned scattering studies of rare gases with squalane and PFPE.[4] For Ne scattering, they find the ratio of the effective surface masses to be $m_s(\mathrm{PFPE}):m_s(\mathrm{squalane}) = 1:0.69$. This same ratio for Ar scattering is 1:0.75, implying that Ar interacts with a larger portion of the squalane surface in impulsive collisions than does Ne. These trends follow the intuitive picture of the hard-cube model, but the liquid surfaces are highly amorphous and dynamic, so caution must be used when employing the extracted effective surface mass values to understand the atomic-level details of energy exchange.

A currently unexplored strategy to separate the individual contributions of mass, structure, and chemical properties of the surface is the use of self-assembled monolayers. Self-assembly of alkanethiols on metal surfaces provides a convenient way to model organic surfaces with control over the molecular-level structure, chemical properties, and mass of the surface.[11] These properties of alkanethiol self-assembled monolayers (SAMs) have enabled detailed studies of rare-gas/organic-surface energy transfer that augment the above-mentioned efforts with organic liquids. Several experiments have investigated the scattering of Ar from a variety of SAMs of different lengths and functionalization at the surface terminus,[12–14] and the scattering of Ne, Ar, and Xe, from regular alkanethiol SAMs.[15–17] Xe scattering off regular SAMs has also been used to induce structural changes in the organic monolayers.[18–20] At a theoretical level, molecular-dynamics simulations have unveiled a wealth of details about the mechanisms governing the scattering of rare gases from SAMs. In particular, Ne/CH_3-SAM simulations have been carried out by Hase and co-workers[21–25] and by Isa *et al.*[15] Ar/CH_3-SAM calculations have been conducted by Bosio and Hase,[26] Gibson *et al.*,[16] and Troya and co-workers,[27,28] and Xe/CH_3-SAM theoretical studies have been carried out by Gibson *et al.*[17]

Recently, CF_3-terminated alkanethiol SAMs have been studied by Lee and co-workers[33] These surfaces have nearly identical structure to the regular CH_3-SAMs, only differing in the chemical composition of the terminal group of the surface. Therefore, comparison of the interfacial behavior of CF_3- and CH_3-SAMs can be used to probe the effect of fluorination on the properties of an organic surface, absent significant structural effects. Lee and co-workers have performed extensive studies of wetting behavior on CH_3- and CF_3-SAMs and find that nonpolar hydrocarbon liquids more readily wet CH_3-SAMs, while polar liquids more readily wet CF_3-SAMs.[29,30] Polar aprotic liquids were not only more wetting on CF_3-SAMs but also displayed an "odd-even" effect as the alkyl chain length was varied. This behavior was attributed to the presence of a strong dipole at the SAM terminus resulting from charge separation in the $-CH_2-CF_3$ moiety. This dipole also influences the surface potential, as evidenced by CF_3-SAMs having a substantially higher frictional response than CH_3-SAMs as measured by atomic force and interfacial force microscopies.[29,31] Studies employing ultraviolet photoelectron spectroscopy have also shown the surface potentials to be measurably different for these two SAMs.[32]

Additionally, Smith *et al.* have investigated CH_3- and CF_3-SAMs using low-energy ion-surface collisions.[33] Replacing the methyl terminus with a trifluoromethyl group results in more efficient conversion of translational energy to internal vibrational modes in the polyatomic probe gases. Further fluorination of the alkyl chains showed minimal additional enhancement of energy transfer, suggesting that interaction with the outermost CX_3 group is most influential in dictating energy conversion.[33] Additional experimental work of energy transfer involving ions compared the results of CH_3-SAMs with a semifluorinated $(CF_3(CF_2)_9(CH_2)_2-SH)$ SAM.[34] Molecular-dynamics simulations have been used to understand the results of ion/CH_3-SAM experiments.[35,36]

The experiments by the Lee and Wysocki groups reveal that fluorination of the terminal methyl unit of alkanethiolate SAMs has a profound effect on the interfacial behavior of the surfaces. In the work described below, we examine the scattering of rare gases from CH_3- and CF_3-SAMs on gold at 60 kJ/mol collision energy to provide an atomic understanding of the distinct properties of these two surfaces. As mentioned above, unlike hydrogenated and fluorinated organic liquids,[1] these organic surfaces have identical structures [other than the slightly different C–X (X=F,H) bond lengths at the CX_3 terminus[29]], and therefore the differences in their interfacial behavior[29–33] can be attributed primarily to the properties of these exposed groups. In particular, we aim to explore the effect of mass on gas/organic-surface energy transfer, which has not been directly and specifically probed in the prior studies with organic liquids. The remainder of this paper is as follows: Details of our experimental and the-

oretical approach are described in Sec. II, the main results of our scattering study are presented in Sec. III, the results are given in-depth discussion in Sec. IV, and our concluding remarks are included in Sec. V.

II. EXPERIMENTAL AND THEORETICAL DETAILS

A. Molecular-beam scattering

As in our previous studies, the SAMs were prepared via spontaneous chemisorption of the corresponding alkanethiol from ~1 mM ethanolic solutions onto clean gold surfaces.[12–14,37] The substrates used in this study were prepared by Au evaporation onto Cr-coated glass slides (EMF Corp.) and were cleaned in Pirahna solution (70% H_2SO_4/30% H_2O_2) prior to use. Previous work using SAMs prepared on both gold-coated glass and gold-coated mica slides found the scattering results to have an insignificant dependence on the underlying substrate used for the monolayer, despite the differences in the polycrystalline structure of the two gold surfaces.[12] Pentadecanethiol ($CH_3-(CH_2)_{14}-SH$) was obtained from Aldrich and used as received. 15,15,15-trifluoropentadecanethiol ($CF_3-(CH_2)_{14}-SH$) was prepared as described by Graupe *et al.* according to established procedures.[38] After immersion in the solutions for at least 24 h, the slides were removed, rinsed with copious amounts of ethanol, dried under a stream of nitrogen, and transferred via a load-lock system into the scattering chamber. The main ultrahigh vacuum (UHV) chamber operates at a base pressure of $<5\times10^{-10}$ torr, which rises to $\sim1\times10^{-9}$ torr during a scattering experiment.

Atomic beams of Ne, Ar, and Kr seeded in either H_2 (Ne) or He (Ar, Kr) were created via standard supersonic expansion techniques.[39] To match the collision energies of each rare gas, we progressively diluted a small volume of the rare gas with H_2 or He, while monitoring the pulsed beam's peak arrival time with a mass spectrometer (Stanford Research Systems) located in the beam path, until we obtained the desired energy. The resulting beams, ~0.5% Ne in H_2, ~0.5% Ar in He, and ~6% Kr in He, yield peak incident energies of 60 kJ/mol (full width at half maximum=17, 11, and 10 kJ/mol for Ne, Ar, and Kr beams, respectively).

Details of our scattering experiment have been presented elsewhere.[12] Briefly, the well-collimated pulsed beam of rare gas (collision energy, E_T=60 kJ/mol) enters an ultrahigh-vacuum chamber containing the SAMs at room temperature. After collision, the recoiling rare-gas atoms are detected with an Extrel mass spectrometer (tuned to m/e=20.0, 40.0, and 84.0 amu for Ne, Ar, and Kr beams, respectively). The spectrometer records the flight times of the rare-gas atoms as they travel from a slotted chopper wheel to the surface and subsequently scatter from the surface into the ionizer. These time-of-flight data are corrected for the chopper-to-surface flight time and other experimental timing offsets. The resulting time-of-flight distribution, $N(t)$, is converted to a final translational-energy distribution using the relation $P(E)\sim t^2N(t)$. Therefore, our experiments measure the amount of energy that the rare gas possesses after collision with the organic monolayer, providing direct information about gas/surface energy exchange.

The beam source and mass spectrometer are geometrically situated such that the angle between the incident beam and the mass spectrometer is fixed (60°). The angle between the atomic beam and the surface normal (incidence angle, θ_i) is 30°, and the surfaces are laser-aligned such that flight times are measured at the specular angle (final angle, θ_f =30°). The collection angle of the mass spectrometer is ±0.5° within the plane of the molecular beam. As our surface mount accommodates two surfaces, we are able to rapidly perform scattering experiments with both the CH_3- and CF_3-terminated SAMs under the same UHV and beam conditions. Switching between the two surfaces requires only a small translation of the manipulator.

B. Molecular dynamics trajectories

To provide insight into the atomic-scale scattering dynamics, we simulated collisions of Ne, Ar, and Kr with both SAMs using classical trajectories. Both CH_3- and CF_3-SAMs form a commensurate $(\sqrt{3}\times\sqrt{3})R30°$ structure, with identical scattering unit cells of 21.5 Å^2 area. The potential-energy surfaces employed to evolve the trajectories have been described in detail in our prior work on Ar+CH_3-SAM collisions.[27,28] Briefly, we divide the potential into two terms: The potential describing the organic monolayer (SAM potential hereafter) and the potential for the rare-gas/SAM interactions (gas/SAM potential hereafter). The optimized potential for liquid simulations force field is used for the SAM, as this standard force field bears out the experimental structure of the SAMs, including a 30° tilt of the chains.[40] The gas/surface potential is described using two-body Buckingham potentials derived from highly accurate *ab initio* calculations of rare-gas/hydrocarbon pairs.[41] Specifically, the intermolecular energies of Ne, Ar, and Kr in various approaches to the CH_4 and CF_4 molecules were calculated at the focal-point coupled-cluster with single, double, and perturbative triple excitations level with extrapolation to the complete basis set limit [fp-CCSD(T)/CBS]. These high-quality points of the intermolecular potential-energy surface were then used to fit pairwise Buckingham potentials. The form of this potential for the interaction between the rare gas and each of the atoms of the SAM is

$$V_{ij}=A_{ij}e^{-B_{ij}r_{ij}}+\frac{C_{ij}}{r_{ij}^6}, \tag{1}$$

where r_{ij} is the internuclear distance between the atoms of each pair, and A_{ij}, B_{ij}, and C_{ij} are adjustable parameters specific to each pair. Table I shows the parameters of the Buckingham potential we employed for all of the pairs involved in the rare-gas/SAM collisions studied in this work. A detailed description of the well depths of each rare-gas/SAM combination will be given in Sec. IV.

Using these potential-energy surfaces, we calculated batches of ~3000 trajectories for each rare-gas/SAM combination unless noted otherwise. For comparison with experiment, the initial angle between the rare-gas' velocity vector and the surface normal (θ_i) was fixed at 30°. The initial conditions of the surface were selected according to a thermal distribution at 300 K. At the beginning of each trajec-

TABLE I. Parameters of the Buckingham potential describing the rare-gas/SAM interactions. (Units are such that if internuclear distances are given in Å, then the potential energy is in kcal/mol.)

	A_{ij}	B_{ij}	C_{ij}
	Rare-gas/CH_3-SAM		
Ne–H	5 663.0	3.732	−77.664
Ne–C	147 236.7	4.312	−158.838
Ar–H	11 426.5	3.385	−374.119
Ar–C	96 594.5	3.608	−356.575
Kr–H	13 754.0	3.238	−621.784
Kr–C	112 927.4	3.520	−268.460
	Rare-gas/CF_3-SAM		
Ne–F	39 879.4	4.510	−128.869
Ne–C	3 408.0	2.934	−297.301
Ar–F	118 267.9	3.907	−579.357
Ar–C	31 219.2	3.297	−230.926
Kr–F	124 268.6	3.721	−872.830
Kr–C	44 043.8	3.210	−304.523

tory, the rare gas was placed 11.5 Å away from the impact point along its incident velocity vector (~10 Å away from the closest surface atom). The trajectories were stopped post-collision when the gas either recoiled to a distance of 12 Å from the closest atom of the surface, or, in the case of long trapping times, after 15 ps. Those trajectories stopped as a result of long trapping times are assumed to have the rare gas fully thermalized with the surface. The rare gas is then randomly assigned a final energy, E_T', based on a Boltzmann distribution at the surface temperature. The percentages of trajectories that do not desorb after 15 ps are 0.6%, 0.0%, 15.4%, 6.9%, 24.2%, and 18.6% for the Ne/CH_3-, Ne/CF_3-, Ar/CH_3-, Ar/CF_3-, Kr/CH_3-, and Kr/CF_3-SAM systems, respectively.

From the initial and final coordinates and momenta of the rare gas, we calculated product translational-energy distributions and scattering-angle-dependent average product energies. Examination of the coordinates and momenta during the trajectory was used to provide mechanistic understanding of the collisions.

III. RESULTS

We show in Fig. 1 the experimental product translational-energy distributions $[P(E_T')]$ for Ne, Ar, and Kr after collision with CH_3- and CF_3-SAMs at E_T=60 kJ/mol with a 30° incidence angle. Figure 1(a) indicates that Ne transfers substantially more energy to the CH_3-SAM than to the CF_3-SAM, suggesting that the more massive surface inhibits energy transfer. The same trend is observed for Ar scattering [Fig. 1(b)], but to a much lesser extent than for Ne. In addition, we see that Ar transfers much more energy to either SAM than Ne. This can be appreciated in the shape of the product translational-energy distribution. In comparing Ne to Ar for either SAM surface, we see that the distributions narrow, with an increase in the low-energy peak and a decrease in the high-energy tail. For Kr [Fig. 1(c)], the difference between CH_3- and CF_3-SAMs reduces even further, such that the energy distributions overlap. We also see that

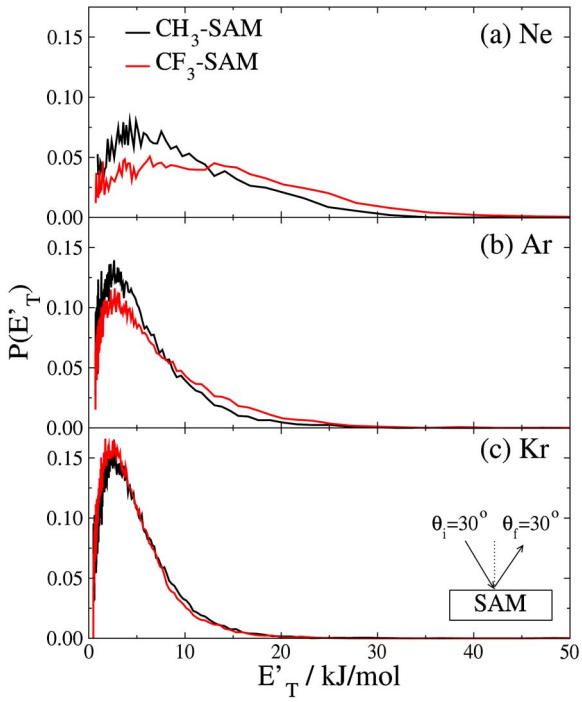

FIG. 1. (Color online) Measured product translational-energy distributions in collisions of rare gases with the indicated SAMs at E_T=60 kJ/mol and θ_i=30°. (a) Ne, (b) Ar, and (c) Kr. The distributions are normalized to unit area.

there is slightly more energy transfer in Kr collisions than in Ar collisions. In effect, the translational-energy distributions become narrower for Kr, with an increase in the low-energy peak that corresponds to enhanced thermalization. Nevertheless, it should be noted that the difference between the product translational-energy distributions for scattering from the two SAMs is much smaller than between the distributions of Ar and Ne.

We show in Fig. 2 the calculated final-energy distributions for the scattering of Ne, Ar, and Kr from the CH_3- and CF_3-SAMs at E_T=60 kJ/mol and θ_i=30°. Although the initial conditions are chosen to match experiments, the total number of simulations that can be performed is limited; therefore, the final-energy distributions in Fig. 2 are integrated over all final scattering angles and scattering planes in contrast with the θ_f=30° detection angle in the in-plane-forward scattering direction used in the experiment. The calculated distributions reproduce the experimental trend: While there is a sizable difference in the scattering of Ne from the CH_3- and CF_3-SAMs, the differences in the amount of energy transferred to the two SAMs decrease with increasing mass of the projectile. For Kr, the distributions for CH_3- and CF_3-SAMs virtually match. For the CF_3-SAM surface, we see that, as seen in the experiment, the product-energy distributions become narrower in the Ne→Ar→Kr sequence. The peak at low energies, which is traditionally attributed to thermal scattering, increases in the same order as observed experimentally for both surfaces.

In an effort to establish direct quantitative comparison between theory and experiment, we have calculated a large batch of Ne+CH_3-SAM trajectories (10 000 total trajectories) and calculated the energy distribution of the Ne prod-

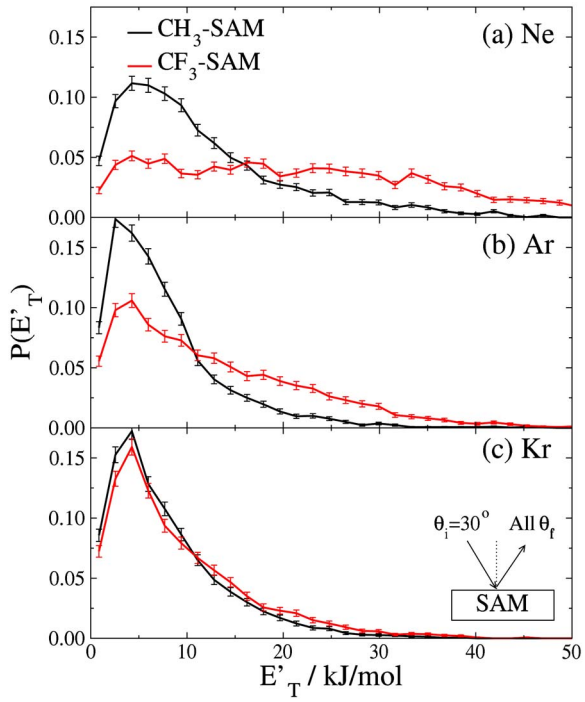

FIG. 2. (Color online) Calculated product translational-energy distributions in collisions of rare gases with the indicated SAMs at E_T=60 kJ/mol and θ_i=30°. (a) Ne, (b) Ar, and (c) Kr. The distributions are normalized to unit area.

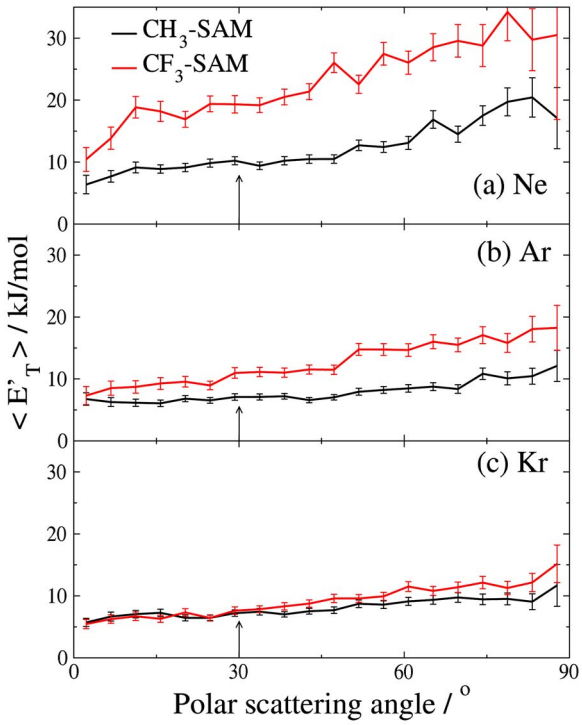

FIG. 4. (Color online) Calculated average product translational energies as a function of the scattering angle in collisions of (a) Ne, (b) Ar, and (c) Kr with CH_3- and CF_3-SAMs at E_T=60 kJ/mol. The arrows correspond to the scattering angle at which the experimental results were obtained.

ucts that scatter in a range of ±10° with respect to the experimental detection polar scattering angle (30°) and within ±30° of the in-plane-forward direction, which is where the detector is located in the experiment. A comparison of these angle-restricted analysis and experiment is displayed in Fig. 3. The figure shows quantitative agreement between theory and experiment. Similar comparisons between angle-restricted calculations and experiment were carried out for the rest of the SAMs with significantly fewer trajectories (~3000). Although the error bars in the calculations are large, we find an overall good agreement between theory and experiment but not always quantitative. These results indicate that the potential-energy surfaces and SAM model used in the simulations adequately mimic the true properties of the systems. Therefore, we can use simulations to provide additional information about the scattering dynamics not readily available from our experimental measurements.

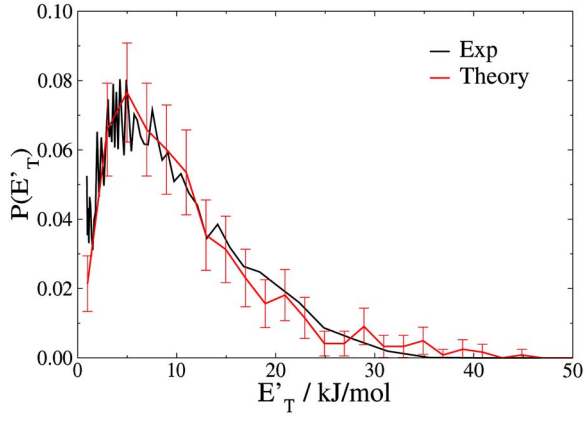

FIG. 3. (Color online) Comparison of measured and calculated product translational-energy distributions in Ne/CH_3-SAM collisions at E_T =60 kJ/mol and θ_i=30°. In the experiments, the energy distributions are measured in the in-plane-forward direction at a polar scattering angle of 30° from the surface normal. The theoretical distribution has been calculated from trajectories scattering in a ±30° window from the in-plane-forward scattering plane and a polar scattering angle in the 20°–40° range. The distributions are normalized to unit area.

To understand further the experimental results, Fig. 4 shows the calculated average product translational energies as a function of the polar scattering angle. The figure reveals that the calculated average energies at θ_f=30° (experimental detection angle) reproduce the experimental trend: The differences in the average energy of the rare gas recoiling from CH_3- or CF_3-SAMs diminish as the mass of the incident gas increases. Much as is seen in the experiments, while the difference between the results of CF_3- and CH_3-terminated SAMs at θ_f=30° is sizable for Ne collisions, the final average product energies overlap for Kr.

Analysis of the calculated polar scattering-angle-dependent product energies in Fig. 4 reveals that the amount of energy transferred to the CH_3- and CF_3-SAMs depends on the final recoil angle of the rare gas. Ne transfers less energy to the CF_3-SAM than to the CH_3-SAM regardless of the scattering angle, and the amount of energy retained by the rare gas increases for larger final scattering angles. For instance, the average energy for near-perpendicular scattering is ~20 kJ/mol smaller than for near-parallel scattering for the CF_3-SAM and ~15 kJ/mol smaller for the CH_3-SAM. In contrast, the amount of energy transferred to both SAMs is essentially the same for Kr scattering and depends very slightly on the final scattering angle. In this case, the differ-

ence between near-perpendicular and near-parallel average final energies reduces to ~10 kJ/mol in the CF_3-SAM and ~5 kJ/mol in the CH_3-SAM. The results for Ar lie nicely between the two extremes of Ne and Kr.

Figure 4 also reveals that energy transfer from the rare gas to the organic monolayer is very efficient. The collisions that exhibit the least energy transfer correspond to Ne scattering from the CF_3-SAM in a direction near perpendicular to the surface normal (parallel to the surface). However, even in this extreme case, Ne transfers on the average about half of its initial translational energy to the SAM. For Kr, only a quarter of the collision energy is retained even when Kr desorbs parallel to the surface. On the other hand, the products desorbing in a direction perpendicular to the surface (parallel to the surface normal) only possess thermal energy at the surface temperature. An exception to this occurs in Ne scattering from the CF_3-SAM surface, where complete thermalization does not seem to be allowed, even when Ne recoils perpendicular to the plane of the surface [Fig. 4(a)].

We have also investigated the dependence of the amount of energy transfer on the azimuthal scattering angle (angle formed by the projections of the initial and final rare-gas velocity vectors on the surface plane). Regardless of the rare-gas/SAM pair, we see that trajectories exhibiting in-plane-forward scattering are associated with minimum energy transfer, as seen before in earlier Ar+CH_3-SAM studies.[27] Specifically, rare gases recoiling in the in-plane-forward direction possess roughly twice more energy than in the in-plane-backward direction for all of the rare-gas/SAM combinations studied in this work. Examination of the azimuthal scattering angle probability distributions indicates that irrespective of the rare-gas/SAM pair, most trajectories undergo in-plane-forward scattering. This result is important because our molecular-beam measurements only detect flux scattered in the in-plane-forward direction.

Further analysis of the simulations reveals that, in accord with previous studies, the gas/surface collisions follow two main mechanisms: Direct impulsive scattering and trapping desorption. To separate these two pathways, we study the dynamics as a function of the number of collisions or encounters between the gas and the surface. We define that an encounter between the gas and the surface takes place when there is a minimum in the coordinate of the rare gas along the surface normal. For the purpose of our analysis, we define that direct impulsive scattering occurs when there is only one minimum on the rare-gas coordinate along the surface-normal axis (i.e., the rare gas hits the surface only once). Figure 5 displays the probability distribution of gas-surface collisions (left axis) and the average product translational energy (right axis), as a function of the number of encounters. Figure 5(a) shows that in most of the Ne collisions (~80%), there is only one encounter between the gas and the surface for both CH_3- and CF_3-SAMs. Therefore, direct impulsive scattering dominates over trapping desorption for both SAM surfaces. Remarkably, the number-of-encounters probability distributions overlap for both SAMs, implying that the difference in the product translational-energy distributions for Ne recoiling from these two SAMs is not due to a change in the number of encounters of the gas with the

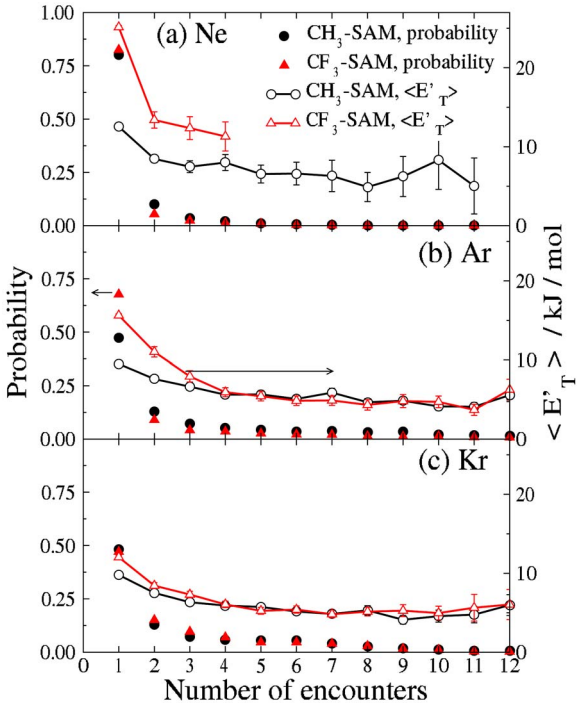

FIG. 5. (Color online) Calculated probability distribution of number of gas-surface encounters (left axis, solid symbols) and average product translational energy (right axis, hollow symbols connected by line) as a function of the number of encounters in collisions of rare gases with the indicated SAMs at E_T=60 kJ/mol. (a) Ne, (b) Ar, and (c) Kr. The arrows in panel (b) are drawn as a guide to the eye. For reference, the average energy of a Boltzmann distribution at the temperature of the surface (298 K) is ~5 kJ/mol.

surface. Instead, Fig. 5(a) shows that the energy transferred per collision determines the outcome. For instance, Ne transfers much less energy (~30% less) to the CF_3-SAM than to the CH_3-SAM in the first encounter. For trajectories that exhibit more than one encounter between Ne and the surface, the energy retained by Ne is significantly larger if it recoils from the CF_3-SAM than from the CH_3-SAM. This result, that Ne transfers less energy to the more massive surface, agrees well with the prediction of elementary hard-cube models that energy transfer decreases with increasing effective surface mass.[42] A more detailed study of the performance of the hard-cube model in rare-gas/SAM collisions is presented later.

Analysis of the mechanism of Ar collisions [Fig. 5(b)] reveals significant differences with respect to Ne. First, Ar has a larger probability of colliding more than once on the SAMs than Ne. Second, Ar has a notably larger probability of experiencing multiple encounters with the CH_3-SAM (~50%) than with the CF_3-SAM (~30%). Therefore, the mechanisms of Ar energy exchange on both surfaces seem to be slightly different. Third, although, as seen in the Ne data, there is less energy transfer from Ar to the CF_3-SAM than to the CH_3-SAM, the amount of energy transferred in the first encounter between Ar and the SAMs is larger than in the case of Ne. For instance, the final average energy of Ne in single-encounter collisions with the CF_3-SAM is ~25 kJ/mol but decreases to ~15 kJ/mol with Ar. For the CH_3-SAM, the average final energy in single-encounter col-

lisions is 12.5 kJ/mol for Ne and 9.5 kJ/mol for Ar. In fact, energy transfer in Ar collisions with SAMs is so much more efficient than with Ne, that Ar is thermalized after three encounters with the CH_3- and CF_3-SAMs [$\langle E_T' \rangle \sim 5$ kJ/mol for four or more encounters, Fig. 5(b)]. In Ne/CF_3-SAM collisions there is no thermalization, and only a very small fraction ($\ll 5\%$) of collisions lead to thermalization of Ne in collisions with the CH_3-SAM [Fig. 5(a)]. These results are in agreement with earlier experiments and calculations of Ne scattering from cold CH_3-SAMs.[15] In that study, the low-energy component of the product-energy distributions could not be well fitted by a Boltzmann distribution at the surface temperature, indicating that full thermalization did not occur. Instead, the distributions were well fitted by a Boltzmann distribution at a temperature significantly higher than the surface temperature. In agreement with those earlier measurements, the Ne/CH_3-SAM product-energy distribution measured in this work at 60 kJ/mol collision energy and 30° incidence in the specular direction can be well fitted by a Boltzmann distribution with $T=660$ K. This result has been recently analyzed in detail by Hase and co-workers. Their extensive trajectory calculations have revealed that trapping desorption is not required to obtain a Boltzmann distribution of product translational energies.[21,22] In effect, the Boltzmann distributions found in Ne scattering off a regular SAM emerge from mostly impulsive collisions.

The results for Ar indicate that the decreased energy transfer of Ar to the CF_3-SAM with respect to the CH_3-SAM is due to (i) an enhanced trapping of Ar on the CH_3-SAM and (ii) a more efficient transfer of energy to the CH_3-SAM than to the CF_3-SAM in single-encounter collisions. Although energy transfer from Ar to the CF_3-SAM is limited in comparison with the CH_3-SAM, it is appreciably more efficient than Ne/CF_3-SAM energy transfer. Therefore, the differences between the final-energy distributions of Ar in collisions with CH_3- and CF_3-SAMs are smaller than those of Ne. As we shall see later, these differences between the scattering of Ne and Ar can be understood mostly as a simple kinematic effect.

For Kr, we find that the microscopic details of the collisions with the CH_3- or CF_3-SAMs are nearly identical. For instance, the number-of-encounters probability distributions [Fig. 5(c)] overlap. This implies that the mechanism of the collisions is the same for both surfaces. The only difference between the two SAMs is that the average energy retained by Kr in single-encounter collisions is slightly larger for the CF_3-SAMs. Figure 4(c) shows that this is due to trajectories in which Kr recoils in a direction nearly perpendicular to the surface normal. At smaller final scattering angles, including the experimental detection angle, the dynamics of Kr/CH_3-SAM and Kr/CF_3-SAM collisions are indistinguishable. The changes in the dynamics when going from Ar to Kr are minor for the CH_3-SAM but notable for the CF_3-SAM. In particular, we see a marked decrease in the probability for single-encounter collisions and an increase in the amount of energy transferred in single-encounter collisions. Therefore, while the differences between the CH_3- and the CF_3-SAMs are appreciable for Ar, they essentially disappear for Kr.

IV. DISCUSSION

In this section, we discuss the origin of the differences in the scattering of Ne, Ar, and Kr from the same organic surface, and the differences in the scattering of the same rare gas from the CH_3- and CF_3-SAMs. Since the structures of the CH_3- and CF_3-SAMs are similar, the differences in the energy transfer dynamics for different rare gases or surfaces must emerge from the change in the collision kinematics (i.e., mass) and/or changes in the gas/SAM and SAM potential-energy surfaces. In the following, we use simulations to address the individual effect of the changes in potential-energy surface with changes in the rare gas or the surface, and the effect of mass.

A. Potential-energy surface effects

To quantify the changes in the rare-gas/SAM potential-energy surface upon changing the rare gas or fluorinating the surface, we examine high-level *ab initio* calculations of rare-gas/CX_4, X=H,F pairs.[41] Focal-point coupled-cluster calculations including single, double, and perturbative triple excitations extrapolated to the complete basis-set limit indicate that the depths of the absolute van der Waals wells of the Y/CH_4 pairs are 0.7, 1.7, and 2.0 kJ/mol for Y=Ne, Ar, and Kr, respectively. The absolute well depths for the Y/CF_4 pairs are 1.1, 2.3, and 2.7 kJ/mol, respectively. Two main conclusions can be extracted from these high-accuracy electronic-structure calculations. First, the long-range attraction between either of the SAMs and the rare gases increases in the Ne→Ar→Kr order, as expected from the increase in polarizability of the rare gases in that order. Second, the interactions of fluorinated alkanes with rare gases are slightly more attractive than those of regular alkanes. This result is also expected from the greater polarizability of fluorocarbons compared to hydrocarbons (i.e., the CF_3- moiety is more polarizable than the CH_3- moiety).

Aside from enhancing the long-range attractions between the gas and the surface, the selective fluorination at the SAM terminus also induces a strong dipole moment in each of the CF_3-SAM chains due to the difference in electronegativity between the terminal $-CF_3$ moiety and the last $-CH_2-$ group of the SAM. Although this surface dipole has been shown to affect the surface free energy,[30] *ab initio* calculations indicate that the interactions between rare gases and CF_3-SAMs are dominated by dispersion interactions, and the effect of the surface dipole is minimal.[41] In particular, the *ab initio* well depth or Ar approaching the fluorinated side of a CH_3CF_3 molecule is identical to the well between Ar and the CF_3CF_3 molecule along the same approach. Analogously, the *ab initio* calculations do not show any difference between the approach of Ar to the hydrogenated side of the CH_3CF_3 molecule or to CH_3CH_3. A force field for fluorocarbons, recently developed from *ab initio* calculations, has also shown that electrostatic terms are not important.[43]

To ascertain whether the changes in the dynamics of Ne, Ar, and Kr scattering off the same surface (Figs. 1 and 2) are due to the changes in the gas/SAM potential-energy surface, we have performed simulations of Ne/CF_3-SAM collisions with two different gas/SAM potentials. Figure 6 shows the

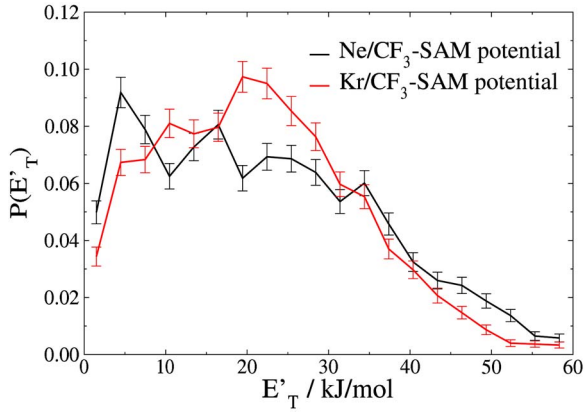

FIG. 6. (Color online) Calculated product-energy distributions in collisions of Ne with the CF_3-SAMs at E_T=60 kJ/mol and θ_i=30° with the indicated gas/surface potentials.

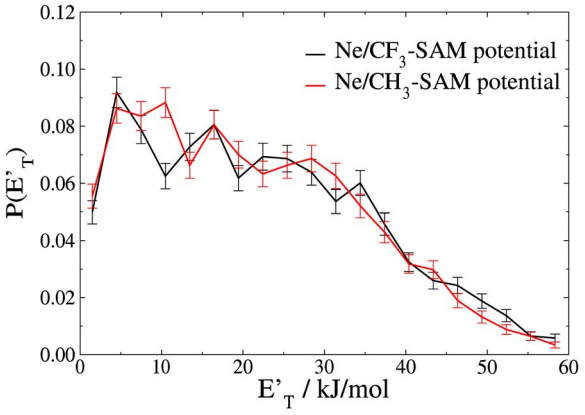

FIG. 7. (Color online) Calculated product-energy distributions in collisions of Ne with the CF_3-SAMs at E_T=60 kJ/mol and θ_i=30° with the indicated global potentials.

product-energy distributions in collisions of Ne with the CF_3-SAM at E_T=60 kJ/mol and θ_i=30° using the regular Ne/CF_3-SAM gas/SAM potentials, and the more attractive Kr/CF_3-SAM gas/SAM potentials. Note that in the simulation involving the Kr/CF_3-SAM potentials, the initial conditions of the trajectories and the mass of the projectile are identical to those of the regular Ne/CF_3-SAM simulations, so the difference in the scattering dynamics is solely due to the gas/SAM potential.

The product-energy distributions of regular Ne/CF_3-SAM collisions and Ne/CF_3-SAM collisions integrated using Kr/CF_3-SAM potentials in Fig. 6 are very similar. Quantitatively, the average fraction of energy transfer $((E_T-\langle E_T'\rangle)/E_T)$ in Ne/CF_3-SAM collisions calculated using the Kr/CF_3-SAM potentials is in good agreement with the result obtained using the regular Ne/CF_3-SAM potentials (0.64 versus 0.62, respectively). These results indicate that the more attractive character of the Kr/CF_3-SAM potential has little influence on the different dynamics of Ne and Kr collisions with SAMs (Figs. 1 and 2). We note that this independence of the potential on the dynamics is likely due to the total collision energy (60 kJ/mol) being much larger than the size of the attractive wells of the potential-energy surfaces. It is expected that at lower collision energies, the differences in the rare-gas/SAM potentials will play a more significant role in the interfacial dynamics.

We now address the effect of the change in the gas/SAM and SAM potential-energy surface upon fluorination on the dynamics of rare-gas/SAM collisions. For this purpose, we have integrated a batch of Ne/CF_3-SAM trajectories at E_T=60 kJ/mol and θ_i=30° in which the gas/SAM potential is artificially set to be that of the Ne/CH_3-SAM, and the SAM potential is set to be that of the CH_3-SAM. Figure 7 shows the product-energy distribution of such simulation compared with the distribution obtained in regular Ne/CF_3-SAM calculations. Both product-energy distributions overlap within statistical uncertainties. Quantitatively, the average fraction of energy transfer in these calculations (0.64) agrees well with the result using the regular gas/surface and SAM potentials (0.62). These results indicate that the changes to both the gas/surface and surface potentials upon fluorination also play a minor role in the dynamics of rare-gas/SAM collisions at the initial conditions explored in this work.

B. Kinematic effects

The above analysis has verified that the differences in the potential-energy surface when changing the rare gas or fluorinating the SAM terminus only have a minor effect on the dynamics. We now focus on determining if kinematic effects alone are responsible for the trends observed in Figs. 1 and 2. We first study the effect of making the surface terminus heavier upon fluorination. To this end, we compare in Fig. 8 the product-energy distributions of Ne scattering at 60 kJ/mol and θ_i=30° from a regular CH_3-SAM and from an isotopomeric SAM in which the mass of the H atoms at the methyl terminus is artificially set to that of F atoms. The gas/surface and SAM potentials are identical in both simulations, and correspond to the potentials for the Ne/CH_3-SAM system. The figure shows a sharp difference in the amount of energy transfer with a change in the mass of the surface terminus. The average fraction of energy transfer with the regular SAM is 0.81 and that with the heavy SAM is 0.64. Also included in the figure is the product translational-energy distribution obtained in the regular Ne/CF_3-SAM simula-

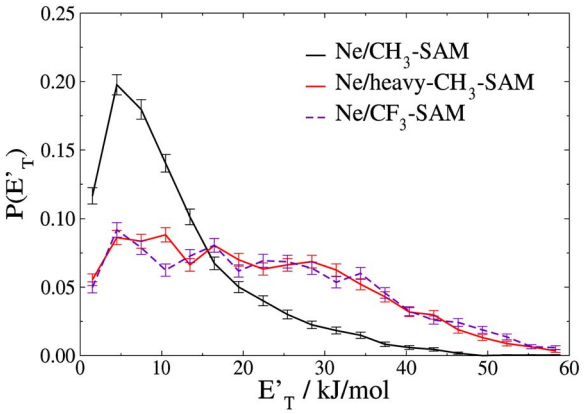

FIG. 8. (Color online) Calculated product-energy distributions in collisions of Ne with the indicated SAMs at E_T=60 kJ/mol and θ_i=30°. The "heavy" CH_3-SAM corresponds to a CH_3-SAM in which the mass of the H atoms of the CH_3 terminus is replaced by that of F atoms in the simulations.

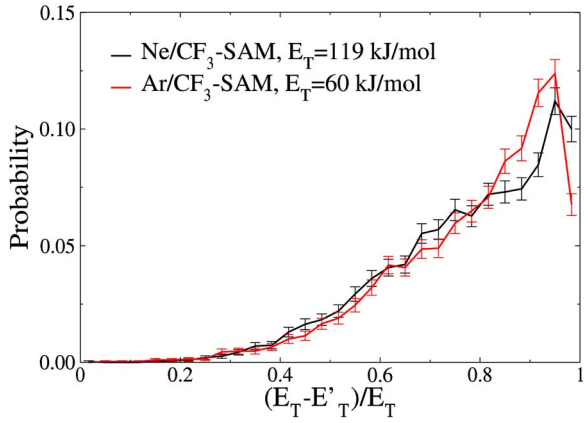

FIG. 9. (Color online) Calculated fraction of energy transfer probability distributions in collisions of Ne and Ar with the CF_3-SAM at E_T = 119 kJ/mol and 60 kJ/mol, respectively. $\theta_i = 30°$. Note that the initial momentum of both rare gases is the same.

tions. The Ne/heavy-CH_3-SAM distribution is in excellent agreement with the Ne/CF_3-SAM distribution. Therefore, a simple change in the mass of the surface terminus greatly limits gas/surface energy transfer in Ne collisions and accounts for the differences between the dynamics of Ne scattering off fluorinated and regular surfaces seen in the experiment [Fig. 1(a)].

To delve further into the effect of kinematics on the dynamics of rare-gas/SAM collisions, we have calculated energy transfer in Ne/CF_3-SAM collisions at 119 kJ/mol and compared it with the Ar/CF_3-SAM results at 60 kJ/mol. In both simulations the rare gas has the same momentum, so the comparison will address the role of initial momentum on gas/organic-surface energy exchange. Figure 9 shows the fraction of energy transfer probability distributions. The distributions are in good agreement with each other, indicating that energy transfer under these two different sets of initial conditions is very similar. The average fractions of energy transfer in Ne/CF_3-SAM collisions at 119 kJ/mol (0.78) and in Ar/CF_3-SAM collisions at 60 kJ/mol (0.79) are also in excellent agreement. We therefore conclude that kinematic effects alone are able to explain the changes in rare-gas/SAM dynamics for different rare gases, and CH_3- or CF_3-SAMs.

The result that mass governs the extent of energy transfer between rare gases and CH_3- and CF_3-SAM surfaces provides a microscopic rationalization of the experimental results in Fig. 1. These results indicate that while there is a large difference in energy transfer to the CH_3- and CF_3-SAMs in collisions of Ne at 60 kJ/mol, these differences essentially disappear for collisions of Kr at 60 kJ/mol. The fact that changes in the gas mass or surface mass alone are able to reproduce this trend suggests the presence of a kinematic barrier for gas/surface energy transfer. In order for a SAM to absorb the energy of an impinging gas-phase species, low-frequency, large-amplitude surface modes need to be excited.[25] These modes are primarily chain wags and torsions, and in order for them to be excited, the SAM chains must move laterally. The excitation received by the SAM is then dissipated to chains adjacent to the impact region. The heavier CF_3-SAM therefore possesses a higher inertial barrier for energy transfer than the lighter CH_3-SAM, as lateral motion of the heavier chains is more difficult. The relatively small momentum of Ne at 60 kJ/mol is not large enough to excite the absorbing modes in the CF_3-SAM as efficiently as in the CH_3-SAM. The lack of efficient Ne/SAM energy transfer in the initial gas/surface collision results in mostly impulsive scattering of the gas. In contrast, the momentum of Kr at 60 kJ/mol is large enough to efficiently excite surface modes in both CH_3- and CF_3-SAM surfaces, even though the CF_3-SAM possesses a higher kinematic barrier for energy transfer. Energy transfer is very efficient in the initial collision, resulting in an increased probability of trapping desorption. The results for Ar scattering lie between those of Ne and Kr: While energy transfer is more efficient than in Ne, the increased inertial barrier for energy transfer to the heavier surface can still be realized.

The fact that changes in the gas or surface mass explain the rare-gas/SAM energy transfer measurements presented in this work offers a great opportunity to calibrate the performance of analytic kinematic models. For instance, the popular hard-cube model[7] has been used extensively in prior studies of gas/organic-liquid energy transfer.[4] This model predicts that energy transfer in impulsive collisions increases with increasing gas mass. It also predicts that an increase in the surface mass decreases the amount of energy transfer in impulsive collisions. The results of our rare-gas/SAM studies validate the prediction of the hard-cube model for the variation of energy transfer with the rare gas. In effect, energy transfer increases in the Ne→Ar→Kr sequence. Regarding the variation of energy transfer with surface mass, we find that the hard-cube model has mixed success. In Ne and Ar collisions, energy transfer diminishes when going from the CH_3-SAM to the heavier CF_3-SAM, which is what the model predicts. However, for Kr, energy transfer to both SAMs is nearly identical even for impulsive (i.e., single bounce) collisions. Within the hard-cube model, this result indicates that the surface masses of the CH_3- and CF_3-SAMs are identical, which is a counterintuitive result. Despite this counterintuitive result, it is surprising that the simple hard-cube model is able to qualitatively capture the major trends of this work considering some of the approximations involved in the model. For instance, the model assumes conservation of the projectile's momentum parallel to the surface, which does not occur in gas/SAM collisions,[15] and the absence of attraction between the gas and the surface, which also disagrees with experiment.

Another failure of the hard-cube model is that it is not able to describe surface penetration. An important result of earlier simulations of collisions of rare gases and other gas-phase species[44,45] with SAMs is that the mechanisms for gas/SAM energy exchange are not limited to impulsive scattering and trapping desorption. Surface penetration by the rare-gas species was seen to be possible in gas/SAM collisions. The simulations carried out in this work reveal that surface penetration by the impinging rare gas at 60 kJ/mol collision energy is important, in particular, for the CH_3-SAM. In this work, we consider that the rare gas has penetrated the surface when it falls 2 Å below the average height of the monolayers. With this definition of surface penetration, we find that at

60 kJ/mol collision energy and 30° incidence angle 15%, 11%, and 19% of the Ne, Ar, and Kr trajectories penetrate the CH_3-SAM, respectively. Interestingly, even though Kr is the largest rare gas studied here, its relatively high momentum allows for an enhanced amount of penetration with respect to Ne and Ar. The percentage of trajectories that penetrate the CF_3-SAM is 17%, 4%, and 6% for Ne, Ar, and Kr, respectively. In this case, the larger kinematic barrier imposed by the heavier terminus of the CF_3-SAM results in substantially less penetration for Ar and Kr with respect to the CH_3-SAM. On the other hand, Ne penetration of the CF_3-SAM is comparable to that of the CH_3-SAM. Therefore, it seems that the small size of Ne allows it to travel similarly through the terminal portion of the CH_3- and CF_3-SAMs.

Analytical models of gas/organic-surface energy transfer more sophisticated than the hard-cube model are available in the literature. In particular, the washboard model of gas/surface scattering developed by Tully[46] has been successfully applied to rare-gas/SAM collisions.[47] Among the merits of this method are the possibility to investigate soft, corrugated surfaces, and the presence of a dependence of energy transfer on the direction and position of the impacts. The detailed experiments and simulations reported in this work will be important to investigate the validity of this more sophisticated model in the future.

V. CONCLUDING REMARKS

The dynamics of energy transfer in collisions of Ne, Ar, and Kr with regular and ω-fluorinated alkanethiolate monolayers have been investigated with the goal of determining the role that mass plays in gas/organic-surface energy transfer. Molecular-beam scattering experiments indicate that while 60 kJ/mol Ne transfers more energy to CH_3-SAMs than to CF_3-SAMs, 60 kJ/mol Kr transfers equal amounts of energy to both organic surfaces. Extensive molecular-dynamics simulations have been carried out to elucidate the microscopic origin of this behavior. The calculated product translational-energy distributions reproduce the experimental trends, lending confidence to the accuracy of the simulations.

High-quality *ab initio* calculations show that the long-range attractions between the rare gases and the SAMs increase in the $Ne \rightarrow Ar \rightarrow Kr$ order, as expected. In addition, ω-fluorination of the SAMs enhances the attractions between the gases and the surface. Molecular-dynamics simulations have been carried out to investigate the effect of the differences in the potential-energy surface on the dynamics. Interestingly, the simulations reveal that the differences in the potential-energy surface play only a minor role in the changing scattering dynamics when going from Ne to Ar and Kr on a particular SAM, and when going from the CH_3-SAM to the CF_3-SAM for a particular gas. Instead, our simulations reveal that changes in the mass of the impinging gas and/or mass of the surface species strongly influence the dynamics of these systems.

The fact that mass governs the extent of energy transfer in collisions of rare gases with CH_3- and CF_3-SAMs therefore enables us to rationalize the experimental finding that Ne transfers different amounts of energy to the CH_3- and CF_3-SAMs, while Kr transfers the same amount of energy to these SAMs. In order for SAMs to absorb energy efficiently from an impinging gas species, the chains of the SAM must move laterally so that neighboring chains can dissipate the energy of the collision. Heavier chains require larger momentum transfer from the colliding gas to exert this lateral motion, which introduces an inertial barrier for energy transfer. The momentum of Ne at 60 kJ/mol is not large enough to displace the CF_3-SAM chains as much as the CH_3-SAM chains, and this results in limited energy transfer to the heavier SAM. Kr at 60 kJ/mol possesses enough momentum to equally excite the absorbing modes of each SAM, and energy transfer for both SAMs is similar. It is found that the popular hard-cube model captures many of the trends measured in the experiments but is not completely predictive. Furthermore, the results highlight that caution must be used when interpreting the effective surface mass calculated in the hard-cube model for gas/SAM collisions.

In the future, it will be important to examine energy transfer from molecules to the model organic surfaces employed in this work. In particular, elucidation of the role played by the internal modes of the gas-phase species on heterogeneous energy transfer will further our understanding of gas/organic-surface collisions.

ACKNOWLEDGMENTS

This work has been supported by the NSF (CHE-0547543 and CHE-0549647) and AFOSR Grant No. FA9550-06-1-0165. The work at the University of Houston was supported by the NSF (DMR-0447588) and the Robert A. Welch Foundation (E-1320). D.T. is a Cottrell Scholar of Research Corporation.

[1] M. E. King, G. M. Nathanson, M. A. Hanning-Lee, and T. K. Minton, Phys. Rev. Lett. **70**, 1026 (1993).
[2] M. E. Saecker, S. T. Govoni, D. V. Kowalski, M. E. King, and G. M. Nathanson, Science **252**, 1421 (1991).
[3] M. E. Saecker and G. M. Nathanson, J. Chem. Phys. **99**, 7056 (1993).
[4] M. E. Saecker and G. M. Nathanson, J. Chem. Phys. **100**, 3999 (1993).
[5] B. G. Perkins and D. J. Nesbitt, J. Phys. Chem. B **110**, 17126 (2006).
[6] M. E. King, M. E. Saecker, and G. M. Nathanson, J. Chem. Phys. **101**, 2539 (1994).
[7] E. K. Grimmelmann, J. C. Tully, and M. J. Cardillo, J. Chem. Phys. **72**, 1039 (1980).
[8] J. N. Smith, Surf. Sci. **34**, 613 (1973).
[9] S. T. Ceyer and G. A. Somorjai, Annu. Rev. Phys. Chem. **28**, 477 (1977).
[10] Y. Watanabe, H. Yamaguchi, M. Hashinokuchi, K. Sawabe, S. Maruyame, Y. Matsumoto, and K. Shobatake, Eur. Phys. J. D **38**, 103 (2006).
[11] J. C. Love, L. A. Estroff, J. K. Kriebel, R. G. Nuzzo, and G. M. Whitesides, Chem. Rev. (Washington, D.C.) **105**, 1103 (2005).
[12] B. S. Day and J. R. Morris, J. Phys. Chem. B **107**, 7120 (2003).
[13] B. S. Day, S. F. Shuler, A. Ducre, and J. R. Morris, J. Chem. Phys. **119**, 8084 (2003).
[14] M. K. Ferguson, J. R. Lohr, B. S. Day, and J. R. Morris, Phys. Rev. Lett. **92**, 073201 (2004).
[15] N. Isa, K. D. Gibson, T. Yan, W. L. Hase, and S. J. Sibener, J. Chem. Phys. **120**, 2417 (2004).
[16] K. D. Gibson, N. Isa, and S. J. Sibener, J. Chem. Phys. **119**, 13083 (2003).
[17] K. D. Gibson, N. Isa, and S. J. Sibener, J. Phys. Chem. A **110**, 1469 (2006).
[18] D. P. Fogarty and S. A. Kandel, J. Chem. Phys. **124**, 111101 (2006).
[19] D. P. Fogarty and S. A. Kandel, J. Chem. Phys. **125**, 174710 (2006).

[20] D. P. Fogarty, N. A. Kautz, and S. A. Kandel, Surf. Sci. **601**, 2117 (2007).
[21] T. Yan, W. L. Hase, and J. R. Barker, Chem. Phys. Lett. **329**, 84 (2000).
[22] T.-Y. Yan and W. L. Hase, Phys. Chem. Chem. Phys. **4**, 901 (2000).
[23] T.-Y. Yan and W. L. Hase, J. Phys. Chem. A **105**, 2617 (2001).
[24] T.-Y. Yan and W. L. Hase, J. Phys. Chem. B **106**, 8029 (2002).
[25] T.-Y. Yan, N. Isa, K. D. Gibson, S. J. Sibener, and W. L. Hase, J. Phys. Chem. A **107**, 10600 (2003).
[26] S. B. M. Bosio and W. L. Hase, J. Chem. Phys. **107**, 9677 (1997).
[27] B. S. Day, J. R. Morris, and D. Troya, J. Chem. Phys. **122**, 214712 (2005).
[28] B. S. Day, J. R. Morris, W. A. Alexander, and D. Troya, J. Phys. Chem. A **110**, 1319 (2006).
[29] M. Graupe, T. Koini, H. I. Kim, N. Garg, Y. F. Miura, M. Takenaga, S. S. Perry, and T. R. Lee, Colloids Surf., A **154**, 239 (1999).
[30] M. Graupe, M. Takenaga, T. Koini, R. Colorado, and T. R. Lee, J. Am. Chem. Soc. **121**, 3222 (1999).
[31] J. E. Houston, C. M. Doelling, T. K. Vanderlick, Y. Hu, G. Scoles, I. Wenzl, and T. R. Lee, Langmuir **21**, 3926 (2005).
[32] D. M. Alloway, M. Hofmann, D. L. Smith, N. E. Gruhn, A. L. Graham, R. Colorado, V. H. Wysocki, T. R. Lee, P. A. Lee, and N. R. Armstrong, J. Phys. Chem. B **107**, 11690 (2003).
[33] D. L. Smith, V. H. Wysocki, R. Colorado, O. E. Shmakova, M. Graupe, and T. R. Lee, Langmuir **18**, 3895 (2002).
[34] J. Laskin and J. H. Futrell, J. Chem. Phys. **119**, 3413 (2003).
[35] O. Meroueh and W. L. Hase, Phys. Chem. Chem. Phys. **3**, 2306 (2001).
[36] O. Meroueh and W. L. Hase, J. Am. Chem. Soc. **124**, 1524 (2002).
[37] B. S. Day and J. R. Morris, J. Chem. Phys. **122**, 234714 (2005).
[38] M. Graupe, T. Koini, V. Y. Wang, G. M. Nassif, R. Colorado, R. J. Villazana, H. Dong, Y. F. Miura, O. E. Shmakova, and T. R. Lee, J. Fluorine Chem. **93**, 107 (1999).
[39] D. R. Miller, in *Atomic and Molecular Beam Methods*, edited by G. Scoles (Oxford University Press, New York, 1988), Vol. 1, p. 14.
[40] J. Hautman and M. L. Klein, J. Chem. Phys. **91**, 4994 (1989).
[41] W. A. Alexander and D. Troya, J. Phys. Chem. A **110**, 10834 (2006).
[42] G. M. Nathanson, Annu. Rev. Phys. Chem. **55**, 231 (2004).
[43] O. Borodin, G. D. Smith, and D. Bedrov, J. Phys. Chem. B **106**, 9912 (2002).
[44] U. Tasic, T.-Y. Yan, and W. L. Hase, J. Phys. Chem. B **110**, 11863 (2006).
[45] E. Martinez-Nunez, A. Rahaman, and W. L. Hase, J. Phys. Chem. C **111**, 354 (2007).
[46] J. C. Tully, J. Chem. Phys. **92**, 680 (1990).
[47] T.-Y. Yan, W. L. Hase, and J. C. Tully, J. Chem. Phys. **120**, 1031 (2004).